Structure and formation mechanism of V defects in multiple InGaN/GaN quantum well layers

M. Shiojiri[a)]
Kyoto Institute of Technology, Kyoto 606-8585, Japan and Department of Anatomy, Kanazawa Medical University, Ishikawa 920-0293, Japan

C. C. Chuo[b)] and J. T. Hsu
Opto-Electronics and Systems Laboratories, Industrial Technology Research Institute, Hsinchu, Taiwan 310, Republic of China

J. R. Yang
Institute of Materials Science and Engineering, National Taiwan University, Taipei, Taiwan 106, Republic of China

H. Saijo
Department of Electronics and Information Science, Kyoto Institute of Technology, Kyoto 606-8585, Japan

(Received 7 October 2005; accepted 10 January 2006; published online 4 April 2006)

A variety of different transmission electron microscopy techniques, and particularly high-angle annular dark-field scanning transmission electron microscopy, has been used to reveal that V defects or inverted hexagonal pyramid defects in multiple InGaN/GaN quantum well (QW) layers nucleate on threading dislocations that cross the InGaN QW. The defects have thin walls lying parallel to $\{10\bar{1}1\}$ with the InGaN/GaN QW structure. A formation mechanism for the V defects is proposed taking into account the growth kinetics of GaN and the segregation of In atoms in the strain field around the cores of the threading dislocations. © *2006 American Institute of Physics*.
[DOI: 10.1063/1.2180532]

I. INTRODUCTION

Functional devices, such as quantum well (QW) lasers, tunneling devices, random access memories, and high-electron mobility transistors, usually comprise nanoscale multilayer heterostructures that exploit quantum confinement effects. GaN and InN have band gaps of 3.4 and 1.9 eV, respectively, and thus $In_xGa_{1-x}N$ materials covering a wide spectral range can be produced by selection of the appropriate value of x. This approach has enabled violet light emitting diodes (LEDs) and laser diodes (LDs) to be fashioned out of InGaN/GaN multiple QWs.[1–3] The lifetime of these diodes can exceed 10 000 h,[4] and they have been widely manufactured for commercial use. Such structures can be produced by epitaxial lateral overgrowth (ELOG) of the GaN layer on a sapphire substrate,[2,3] followed by deposition of a AlGaN/GaN strained-layer superlattices (SLS) cladding.[5–7] The ELOG and SLS prevent dislocations or nanopipes from forming due to mismatch between the Al_2O_3 and GaN lattices, and between the GaN and AlGaN lattices, respectively, thereby reducing the densities of threading defects that propagate to the multiple InGaN/GaN QW layer through the substructures. Our recent high-angle annular dark-field (HAADF) scanning transmission electron microscopy (STEM) observations of n-$Al_{0.14}Ga_{0.86}N$ (3 nm)/n-GaN(3 nm) SLS clearly distinguished between the AlGaN and GaN layers and accurately positioned dislocations in the SLS.[8,9] We found that the SLS significantly reduced the number of threading dislocations (TDs) reaching the multiple QW (MQW) layer. In spite of these advances, defect-free multiple InGaN/GaN QW layers have not yet been obtained. This can be mainly ascribed to the very high-equilibrium vapor pressure of nitrogen and the large mismatch between InGaN and GaN lattices. In order to eliminate the threading defects completely, it is essential to understand their structures and formation mechanisms.

TDs form on the interfaces between the underlying GaN layer for the MQW and the nucleation layer on the sapphire substrate, and extend along the c axis growth direction towards the MQW.[10–12] *Inverted hexagonal pyramid* (IHP) *defects* or *V defects* can form at the TDs in the multiple InGaN/GaN QW layer.[13–16] The names originate from the fact that empty pyramidal pits, with hexagonal openings at the growth surface and sidewalls parallel to $\{10\bar{1}1\}$ planes, are formed during the MQW growth.[14] These are subsequently filled during growth of the p-type GaN capping layer to form an IHP.[15] Two different structural models have been proposed for the $\{10\bar{1}1\}$ sidewalls of the IHPs; one is that the sidewalls include thin InGaN/GaN layers,[13] the other is that the InGaN quantum wells end abruptly at the surfaces of the pits and these are then filled by the GaN capping layer with no InGaN/GaN sidewall layers.[14–16] This fundamental issue has not been resolved because it is very hard to perform an atomic-scale structural or compositional analysis of such ultrathin layers even by conventional analytical high-resolution transmission electron microscopy (HRTEM).

Recently, we have observed a thin six-walled structure

[a)]Present address: 1-297 Wakiyama, Enmyoji, Kyoto 618-0091, Japan; electronic mail: shiojiri@pc4.so-net.ne.jp
[b)]Author to whom correspondence should be addressed; electronic mail: ccchuo@itri.org.tw

 © 2006 American Institute of Physics

Downloaded 11 Sep 2008 to 140.112.113.225. Redistribution subject to AIP license or copyright; see http://jap.aip.org/jap/copyright.jsp

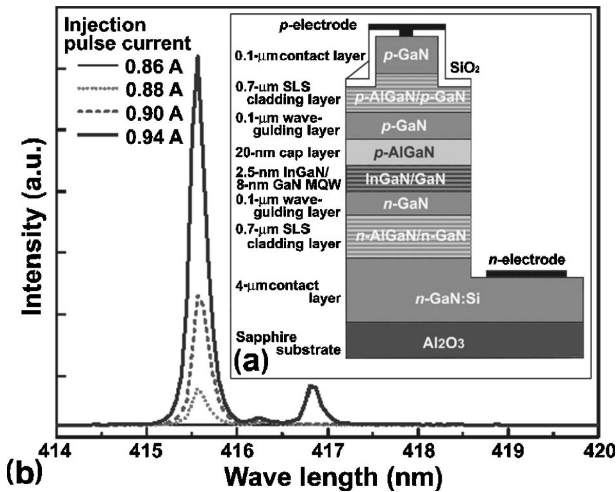

FIG. 1. GaN-based violet laser diode. (a) Structure of a standard laser diode showing the position of a multiple InGaN/GaN QW layer and $Al_{0.14}Ga_{0.86}N$/GaN SLS cladding layers. (b) Room temperature emission spectra of the 10 μm $\times$ 1000 μm ridge-waveguide laser diode measured under pulsed operation. At the injection pulse current above the threshold current of 870 mA, a strong stimulated emission appears at 415.5 nm with a full width at half maximum (FWHM) of 0.2 nm, together with two small peaks between 416 nm and 417 nm (Ref. 19).

consisting of InGaN/GaN $\{10\bar{1}1\}$ layers in the V defects using HAADF-STEM[17] and field-emission gun scanning electron microscopy (FEG-SEM) imaging.[18] These observations support the model suggested by Wu *et al.*[13] In this paper, we present a more detailed analysis of HAADF-STEM, HRTEM, and FEG-SEM data on the structure of the V defects in multiple InGaN/GaN QW layers; these data give definitive evidence for the formation mechanism of the V defects.

II. EXPERIMENTAL PROCEDURE

Samples were prepared by successive metalorganic vapor-phase epitaxy (MOVPE) depositions of (1) an undoped GaN nucleation layer at 550–570 °C on a (0001) sapphire substrate, (2) an undoped GaN layer at 1150 °C, (3) an n-GaN:Si underlying layer (approximately 2 μm) at 1150 °C, (4) multiple $In_xGa_{1-x}N$/GaN QW layers at 820–870 °C, and (5) a capping layer of GaN or AlGaN at 1150 °C. The final structures were similar to that of the prototype wafer of a violet LD structure shown in Fig. 1(a), which displays the positions of the InGaN/GaN QW layer and AlGaN/GaN SLS cladding layers. The LD had demonstrated a strong emission peak at about 415.5 nm with two small peaks between 416 nm and 417 nm, as shown in Fig. 1(b).[19,20] For these studies, some of the samples were deposited without SLS claddings to enable us to investigate the effects of the TDs. The specimens for HAADF-STEM and HRTEM were prepared by mechanical polishing, followed by ion milling. The specimens for FEG-SEM were prepared by cleaving the sapphire substrate with the epilayers, and cross-sectional surfaces were observed directly without any surface treatment. FEG-SEM observations were performed in a Hitachi S-5200 instrument, which gives a resolution of 1.8 nm at 1.0 kV and 0.5 nm at 30 kV. HAADF-STEM and HRTEM observations were performed in a Tecnai F30, equipped with a supertwin objective lens pole-piece (spherical aberration coefficient, Cs, =1.2 mm), and operated at 300 kV. The HAADF-STEM images were recorded using a detector range of D=36–190 mrad, using a convergent electron probe with a semiangle of α=26 mrad. All of the HAADF-STEM, HRTEM, and FEG-SEM images presented in this paper are in their original state (i.e., without any image processing).

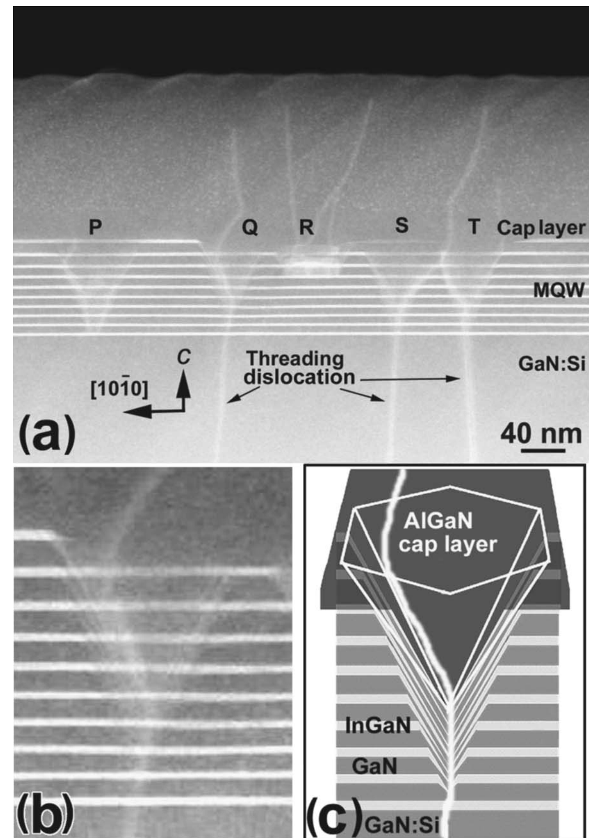

FIG. 2. (a) HAADF-STEM image of a capped $In_{0.2}Ga_{0.8}N$ (2.5 nm)/GaN (8 nm) QW layer grown on the GaN:Si layer, obtained with the beam direction parallel to $[\bar{1}2\bar{1}0]$. The ten bright stripes parallel to the basal plane are the $In_{0.2}Ga_{0.8}N$ QW layers. Both the threading dislocations lying approximately parallel to the c axis and the V defects appear as bright contours. (b) Enlarged image of the V defect at Q in (a). The V defect grew in the form of a thin six-walled structure with thin InGaN/GaN $\{10\bar{1}1\}$ layers. (c) Schematic diagram of the structure of the V defect, which nucleates at a threading dislocation in the first $In_{0.2}Ga_{0.8}N$ QW. The threading dislocation propagates to the free surface through the filled V defect.

III. RESULTS AND DISCUSSION

Figure 2(a) shows a cross-sectional HAADF-STEM image of a multiple $In_{0.2}Ga_{0.8}N$/GaN QW layer with the GaN:Si underlying layer, taken with the beam direction parallel to the a_2 axis in the GaN. The nominal thicknesses of the $In_{0.2}Ga_{0.8}N$ QWs and the GaN barrier layers were 2.5 and 8 nm, respectively. HAADF-STEM images exhibit strong Z contrast[21] that depends on the atomic number, mainly due to thermal diffuse scattering of electrons or incoherent imaging of elastically scattered electrons,[22] unlike conventional transmission electron microscopy (CTEM), which utilizes coherent imaging of elastically scattered electrons. Since indium (Z=49) gives rise to a higher diffuse scattering intensity than

Downloaded 11 Sep 2008 to 140.112.113.225. Redistribution subject to AIP license or copyright; see http://jap.aip.org/jap/copyright.jsp

gallium ($Z=31$), the ten bright stripes observed parallel to the basal plane can be identified as the $In_{0.2}Ga_{0.8}N$ QWs.[23] The TDs propagate along the c axis through the GaN:Si layer and appear as brighter contour lines. The random static atomic displacements around dislocation cores also give rise to diffuse scattering, similar to the thermal diffuse scattering, and consequently causes strong intensity in HAADF-STEM images.[21] Hence, the bright contour lines indicate the exact position of the TDs, unlike diffraction contrast dislocation images in CTEM. Bright V-shaped contours are also seen in the image. They are images of the V defects, whose structure is discussed in the next paragraph. In each case, the apex of the V defect corresponds to the position at which a TD crosses an $In_{0.2}Ga_{0.8}N$ QW (in most cases in the first one). The TD propagates to the free surface through the V defect, as reported by Wu *et al.*[13] and Sharma *et al.*[15] It should be noted that the lateral extent of the V defects is larger than the TEM sample thickness, so in most cases cross-sectional images such as Fig. 2(a) show only a portion of the defect. For example, in the V defect labeled Q, some of the upper parts of the walls are lost together with the tenth QW. In this case we estimate the thickness of the specimen to be about 80 nm ($=2d/\sqrt{3}$) from the length $d=70$ nm of the base of V. The TD associated with the V defect labeled P was presumably removed during the thinning process, while the tenth QW is seen on the base of the V defects labeled S and T whose TDs were located close to one another, and the feature labeled R consists of three overlapping V defects.

An enlarged image of the V defect labeled Q in Fig. 2(a) is reproduced in Fig. 2(b), wherein several inclined brighter stripes can be seen, especially on the left-hand side of the V. These thin stripes terminate on horizontal InGaN QWs, successively decreasing the number of the sidewall stripes with increasing height in the V. The apical angle of the V is approximately 56°, which corresponds to the angle between the $(10\bar{1}1)$ and $(\bar{1}011)$ planes. Thus, the thin bright stripes on the sidewalls would be InGaN layers on $(10\bar{1}1)$ and $(\bar{1}011)$ planes. This result supports the structural model proposed by Wu *et al.*,[13] in which the V defect includes the buried sidewall QWs on the $\{10\bar{1}1\}$ planes and the open hexagonal inverted pyramid that is defined by the six $\{10\bar{1}1\}$ planes and filled with capping matrix afterward. The structure of the V defect is illustrated in Fig. 2(c), showing six symmetric $\{10\bar{1}1\}$ planes with thin QWs and the corresponding TD. Hence, the Z contrast in the HAADF-STEM image gives the definitive evidence for the sidewall QWs of the V defect, although Wu *et al.*[13] did not indicate any persuasive microscopy image. Rather, a CTEM image shown by Romano and Northrup is illustrative.[24] We can conclude that these sidewall InGaN/GaN QWs are an origin of undesirable long-wavelength small emissions like the emissions between 416 nm and 417 nm caused in the 415-nm LD shown in Fig. 1(b). Sharma *et al.*[15] have claimed that the horizontal InGaN QWs end abruptly at the interfaces of the V defects, based upon evidence obtained using a number of complementary EM techniques including HAADF-STEM. We note, however, that HAADF-STEM was used only to verify the structure of the flat horizontal MQWs in their samples, rather than for investigating the sidewall structure. Their conclusion that the V defect is filled with capping materials without InGaN/GaN sidewalls was based upon data from energy-filtered TEM mapping and x-ray mapping, but the sensitivity and resolution of these techniques may be too low to detect the ultrathin sidewall InGaN and GaN layers.

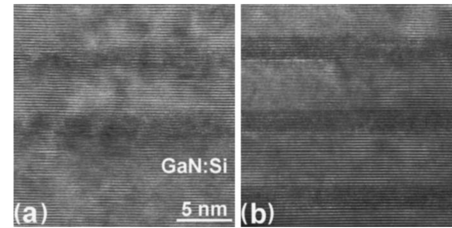

FIG. 3. (a) and (b) HRTEM images of $In_{0.2}Ga_{0.8}N$/GaN QWs in the same sample as shown in Fig. 2, obtained with the beam direction parallel to $[\bar{1}2\bar{1}0]$ at around Scherzer focus. Darker bands parallel to the basal plane are the InGaN QWs. The $In_{0.2}Ga_{0.8}N$ layers in (a) are the first and second QWs.

Figure 3 shows two examples of HRTEM images obtained from $In_{0.2}Ga_{0.8}N$ (2.5 nm) QWs and GaN (8 nm) barrier layers at Scherzer defocus. The $In_{0.2}Ga_{0.8}N$ QWs appear as darker bands and the interfaces between the QWs and GaN layers are rather indistinct in places. Moreover, there appears to be some deformation of the crystal lattices in the first and second QWs in Fig. 3(a). This deformation may be correlated with a V defect, but it is difficult to draw definitive conclusions because the contrast in HRTEM images is greatly influenced by small lattice distortions and compositional changes. Furthermore, the TDs could not be recognized in the HRTEM images because since most of TDs are pure-edge dislocations ($b=1/3\langle 11\bar{2}0\rangle$) the lattice images taken in the $[\bar{1}2\bar{1}0]$ can hardly detect them. HRTEM certainly shows that the interfaces between the $In_{0.2}Ga_{0.8}N$ and GaN lattices are coherent, as seen in Figs. 3(a) and 3(b), but it is not as useful as HAADF-STEM imaging for structural analysis of the V defects.

Further observations were carried out using high-resolution HAADF-STEM. Figure 4 shows an atomically resolved HAADF-STEM image of an $In_{0.2}Ga_{0.8}N$ QW between

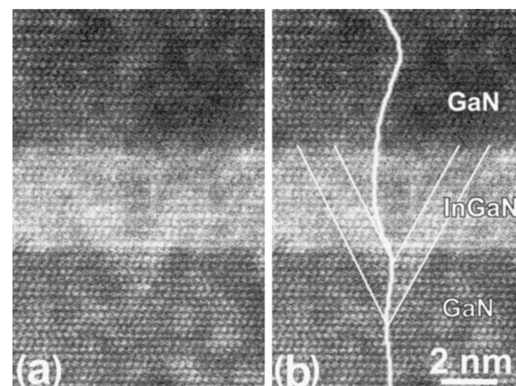

FIG. 4. (a) High-resolution HAADF-STEM image of an $In_{0.2}Ga_{0.8}N$ QW between the GaN barrier layers in the same sample as shown in Fig. 2, obtained with the focused beam direction parallel to $[\bar{1}2\bar{1}0]$ at around Scherzer focus. (b) The same image with lines added to indicate the positions of the sidewall QWs on the $(10\bar{1}1)$ and $(\bar{1}011)$ planes in the V defect, and the incorporated TD.

Downloaded 11 Sep 2008 to 140.112.113.225. Redistribution subject to AIP license or copyright; see http://jap.aip.org/jap/copyright.jsp

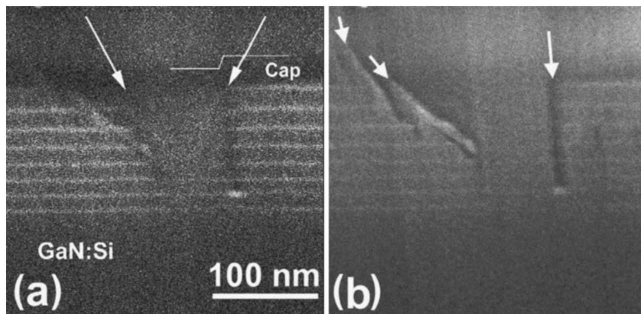

FIG. 5. (a) Backscattering electron image of a capped multiple $In_{0.25}Ga_{0.75}N$(2.5 nm)/GaN(13.9 nm) QW layer grown on the GaN:Si underlying layer, obtained with the beam direction parallel to $[\bar{1}2\bar{1}0]$. Arrowheads indicate the position of a V defect. (b) Secondary electron image of the same area. Arrowheads indicate the position of surface defects, which were caused by cleaving the sample wafer to prepare the SEM specimen. These two images were taken at an accelerating voltage of 10 kV.

the GaN barrier layers in the same sample. The $In_{0.2}Ga_{0.8}N$ QW exhibits strong intensity, showing distinctly the difference in composition from the GaN. In spite of the noise in this image we can see the brighter sidewall QWs on the $(10\bar{1}1)$ and $(\bar{1}011)$ planes and the darker inside of the V defect as compared with the matrix QW, and these are indicated in Fig. 4(b). Away from this V defect, Fig. 4(a) shows that the QW lattice was apparently coherent with the GaN barrier lattice. That is, the lattice in the $In_{0.2}Ga_{0.8}N$ QW as thin as a few nanometers (in this case the nominal thickness was 2.5 nm but the thickness estimated from the image was approximately 3.6 nm, corresponding to 14 monolayers) was strained to match the GaN lattice on the (0001) interfaces. Complementarily, the $In_{0.2}Ga_{0.8}N$ lattice was, as a whole, extended along the c axis. In addition, there was local fluctuation of expansion, which corresponded to local fluctuation of an In atom in the $In_{0.2}Ga_{0.8}N$ QW.[25] The In-rich regions, considered as quantum dots, caused large expansion along the [0001] direction.

Figure 5(a) shows a backscattered electron SEM image of a multiple $In_{0.25}Ga_{0.75}N$(2.5 nm)/GaN(13.9 nm) QW layer grown on the GaN:Si layer, taken using a yttrium aluminum garnet (YAG) detector at an accelerating voltage of 10 kV. Figure 5(b) is the corresponding secondary electron SEM image. The secondary electron image gives topographic contrast from the specimen surface, while the backscattering image, which is mainly due to Rutherford backscattered electrons, provides composition information. In Fig. 5(a), the bright stripes are from the $In_{0.25}Ga_{0.75}N$ QWs, and a V defect, indicated by arrowheads, is detected. The contrast of the V defect can be distinguished from defects on the specimen surface, caused by cleaving, by comparing the contrast with that in Fig. 5(b). The V defect has its apex in the first horizontal QW and leaves its trace as steps on the surface of the capping layer. We can also see the thin QWs on the sidewalls, particularly on the left-hand side of the defect. The 10-keV incident electrons penetrate to about 350 nm, and the backscattering of the electrons occurs at atoms within a depth of about 150 nm, with a maximum at about 100 nm below the surface. Therefore, the backscattering electron image reveals the compositional variation within a depth of ~150 nm but lattice-displaced defects such as threading defects would not be detected. The advantage of these SEM observations is (1) the simple specimen preparation without a risk of any structural changes such as those which might be caused during the thinning treatments that are necessary for TEM and STEM specimens, and (2) the ability to distinguish compositional effects from topological effects, such as surface steps and lattice distortion, by comparing backscattered electron and secondary electron images.

Regarding the formation of the V defects, Chen *et al.*[14] assumed that they were initiated by local In segregation in Cottrell atmospheres around the dislocation cores, which inhibits the crystal growth. They explained that Frank's mechanism, wherein the total energy of the highly strained lattice around a dislocation having a large Burgers vector can reduced by changing the filled core to a hollow open pipe,[26] cannot explain the formation of V defects, because of (1) the cone shape, instead of a tube of constant width along the dislcation core as predicted by Frank; (2) the formation only in the InGaN QWs, in spite of the propagation of the dislocation through both InGaN and GaN layers; and (3) the dramatic change of the pit densities from GaN to InGaN. According to Wu *et al.*,[13] who predicted the sidewall QWs on the $\{10\bar{1}1\}$ planes and the propagation of TDs to the free surface through the capping layer, the primary cause of the V-defect growth is not strain relief, but rather the reduced Ga incorporation (and thus growth rate) on the $\{10\bar{1}1\}$ planes in comparison with the (0001) plane.

Northrup and Neugebauer[27] performed first-principles calculations of the energies for a number of low-index In-terminated GaN surfaces, and showed that In behaves as a differential surfactant, reducing the energy of the $\{10\bar{1}1\}$ surfaces relative to (0001), and enabling the formation of the V defect. They used Frank's model to calculate the formation energy of the V defect, taking the TD to be a screw dislocation with a small open core. We note, however, that this assumption is not consistent with experimental observations which indicate that most of the TDs are not screw dislocations ($b=[0001]$) but are edge dislocations ($b=1/3\langle 11\bar{2}0\rangle$). The energies of these edge dislocations will be approximately 3/8 those of the screw dislocations used in their calculation, if we take the energy to be proportional to the square of the Burgers vector. Sharma's missing of the sidewall MQWs[15] seems to have been caused by impression of their calculation, which may lead to the abrupt ending of the InGaN QWs at the V-defect interfaces. Their calculation also implies that the TDs terminate at the apex and thus disappers within the V defect filled with the cap layer. However, as shown in Fig. 2, the TD appears within the V defect and propagates to the free surface; this is also consistent with the images presented by Romano and Northrup,[24] Wu *et al.*,[13] and Sharma *et al.*[15]

Under MOVPE growth conditions such as those used in the present experiments, the GaN layers grown at a high temperature (~1100 °C) usually exhibit the Ga-terminated (0001) surfaces.[28] This surface is terminated with Ga atoms because the dangling bond density of Ga atoms is a third of that of N atoms, as shown in Figs. 6(a) and 6(b). Hiramitsu *et*

Downloaded 11 Sep 2008 to 140.112.113.225. Redistribution subject to AIP license or copyright; see http://jap.aip.org/jap/copyright.jsp

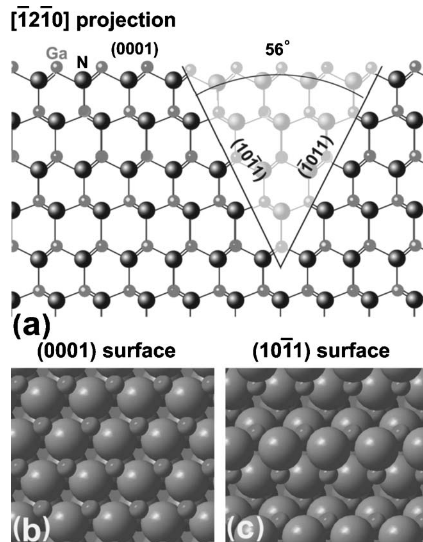

FIG. 6. (a) Projection of the GaN crystal structure along $[\bar{1}2\bar{1}0]$. All of the EM images presented in this paper were obtained with the beam direction parallel to this axis. The orientations of the $(10\bar{1}1)$ and $(\bar{1}011)$ planes are indicated in this projection to show the configurations of the side walls for the V defects observed in this study. (b) Schematic diagram of the (0001) GaN surface terminated by Ga atoms: the dangling bond density is 11.4. (c) Schematic diagram of a $\{10\bar{1}1\}$ surface terminated by N atoms; the dangling bond density is 16.0.

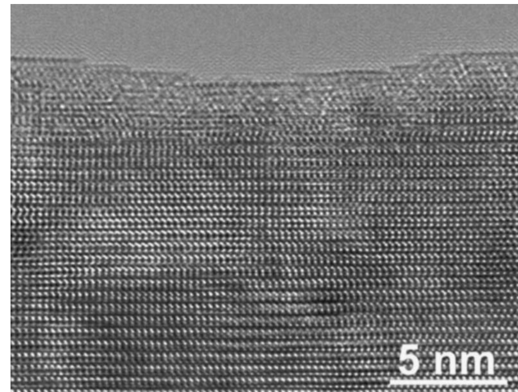

FIG. 7. HRTEM image of the capping GaN layer deposited on the $In_{0.2}Ga_{0.8}N/GaN$ MQW heterostructure. Steps on the outer surface are an effect of V defect in the MQW layers.

al.[29] investigated the effect of the reactor pressure and temperature on the GaN formed by ELOG, which gives us a hint for the V-defect formation. According to them, the ELOG GaN exhibits $\{10\bar{1}1\}$ facets, which are terminated with N atoms as shown in Figs. 6(a) and 6(c), at a lower temperature (or higher reactor pressure) because the N surface is stabilized at the lower temperature under the growth condition of high V/III source gas ratio, such as MOVPE. On the contrary, the $\{10\bar{1}1\}$ facets become unstable at a higher temperature (or lower pressure) because the surface nitrogen atoms are not stabilized. As a result, the grown GaN crystals have the (0001) facet, which are energetically more favorable. The enhanced surface migration of Ga atoms allows the layer-by-layer growth, resulting in a smooth (0001) surface during the high-temperature growth. In other words, the growth rate of the $\{10\bar{1}1\}$-N surfaces decreases and that of the (0001)-Ga surfaces increases with decreasing reactor temperature (or increasing reactor pressure).

The GaN:Si underlying layer in our sample grew at a high reactor temperature of 1150 °C, layer by layer keeping the smooth (0001) surface, although it included several TDs. To suppress reevaporation of In, the multiple InGaN/GaN QW layer was deposited at a reactor temperature as low as 820 ~ 850 °C; for which the poor surface diffusion of Ga atoms, and particularly In atoms, might impede the layer-by-layer growth. In fact, the typical growth rate of InGaN/GaN layer was ~3.3 nm/min. If any mask were placed on the underlying GaN:Si surface, the InGaN/GaN MQW layer would grow with the $\{10\bar{1}1\}$ facets, similar to GaN crystals formed by ELOG at the same temperature. The formation of the V defects can be explained by analogy with the ELOG. Indium atoms, as a foreign element, play an important part in the formation of the V defect, making the small mask (the nucleus of the V defect) by trap and segregation in the strained field around the core of a TD (or Cottrell atmosphere). The mask hinders Ga atoms from migrating on the (0001) monolayer to make a smooth monolayer, and then causes the termination on the six $\{10\bar{1}1\}$ planes of the InGaN and GaN layers successively grown, which become the sidewalls of the forming V-shaped pit. During successive MOVPE the layer growth also occurs on the new surfaces of the six $\{10\bar{1}1\}$ sidewalls, although the growth rate is slower compared with the (0001) face, and consequently the observed thin sidewall InGaN and GaN layers are formed. The unburied V pit is filled with the capping layer material deposited at the high temperature of 1150 °C, whose lattice is connected on the $\{10\bar{1}1\}$ interface, coherently with the lattice of thin InGaN or GaN layers [see Figs. 2(c) and 4]. A trace of the retardation of the growth which occurred within the V pit during the InGaN/GaN deposition can be seen as steps on the final surface in Fig. 7 and also in Fig. 5(a). When the materials in the V defect are buried with the coherent lattice relation to the matrix InGaN/GaN QWs, the V defect has the same cellular structure as that of the GaN:Si just below the V defect. Then, the TD incorporated with the V defect appears as the survivor within the V defect and is taken over in the upper layer. We previously found that V defects start even at In-rich dots in the QW,[17] and also found that the In-rich regions correspond with lattice expansion along the c axis.[25] The wide In-rich region might behave as a masking effect. In this formation mechanism, which supports Wu *et al.*[13] and Chen *et al.*,[14] In atoms help the nucleation of the V defect but the formation of the six $\{10\bar{1}1\}$ sidewalls is ascribed to the growth kinetics of the GaN crystal, independently of the presence of In atoms. In fact, we have detected no V defects in a cladding layer comprised of 200 couple layers of a strained $Al_{0.14}Ga_{0.86}N$ (3 nm) and GaN (3 nm) superlattice grown at 1150 °C on the GaN:Si underlying layer, although we have observed TDs.[8,9]

IV. CONCLUSION

We have observed InGaN/GaN QWs by HAADF STEM, HRTEM, and FEG-SEM, and established the structure and formation mechanism for the V defects in the QWs.

Downloaded 11 Sep 2008 to 140.112.113.225. Redistribution subject to AIP license or copyright; see http://jap.aip.org/jap/copyright.jsp

(1) The specimens used were a ten $In_{0.2}Ga_{0.8}N$ (2.5 nm)/GaN (8 nm) QW layer and an eight $In_{0.25}Ga_{0.75}N$(2.5 nm)/GaN(13.9 nm) QW layer, deposited at a reactor temperature of 820–850 °C on an underlying GaN:Si layer grown at 1150 °C. The QW layers were capped with a GaN or AlGaN layer deposited at 1150 °C.

(2) In these MQW layers, V defects were observed nucleating on TDs crossing the InGaN QW just above the underlying layer. HAADF-STEM gave unequivocal evidence that the V defects have a thin six-walled structure corresponding to InGaN/GaN QWs on $\{10\bar{1}1\}$, and this was confirmed by backscattered electron imaging in FEG-SEM.

(3) HRTEM and high-resolution HAADF-STEM images revealed that the interfaces between the InGaN QWs and the GaN layers are coherent both on $\{10\bar{1}1\}$ and (0001), to make the same cellular structure as a whole.

(4) The TD incorporated with the V defect propagated to the free surface through the V defect buried with the cap layer.

(5) On the basis of these observations we explained the formation of the V defect, taking into account the growth kinetics of the GaN crystal and a masking effect of In atoms. The growth rate of the $\{10\bar{1}1\}$ surface decreases at a temperature as low as 820–850 °C used for the deposition of the InGaN/GaN QW layer. Then, if a mask disturbing the (0001) layer growth is formed, the termination would occur on the six $\{10\bar{1}1\}$ planes of the InGaN and GaN layers successively grown, which become to the sidewalls of the forming V-shaped pit. Indium atoms trapped and segregated in the strained field around the core of a TD play a role as a small mask, hindering Ga atoms from migrating on the (0001) monolayer to make a smooth (0001) monolayer.

ACKNOWLEDGMENTS

The authors thank K. Inoke and E. Kobayashi, FEI Company, Japan, for taking HRTEM and HAADF-STEM images, M. Nakagawa and Dr. M. Yamada, Hitachi Science Systems, for taking FEG-SEM images, and Professor M. Aindow, University of Connecticut, for critical reading of the manuscript. One of the authors (M. S.) thanks Dr. K. Watanabe and Dr. T. Yamazaki, Tokyo University of Science, for discussions at the early stage of this work. Thanks are due to T. C Wang and C. E. Tsai for assistance with MOCVD growth, which was supported financially by the Ministry of Economic Affairs of Taiwan, R.O.C. under Project No. B341AB8111.

[1] S. Nakamura, M. Senoh, S. Nagahama, N. Iwasa, S. Saito, T. Mastusita, Y. Sugimoto, and H. Kiyoku, Appl. Phys. Lett. **69**, 4056 (1996).
[2] A. Usui, H. Sunakawa, A. Sasaki, and A. Yamaguchi, Jpn. J. Appl. Phys., Part 2 **36**, L899 (1997).
[3] O. H. Nam, M. D. Bremser, T. Zheleva, and R. F. Davis, Appl. Phys. Lett. **71**, 2638 (1997).
[4] S. Nakamura, M. Senoh, S. Nagahama, T. Mastusita, H. Kiyoku, S. Sugimoto, T. Kozaki, H. Umemoto, M. Sano, and T. Mukai, Jpn. J. Appl. Phys., Part 2 **38**, L226 (1999).
[5] S. Nakamura, M. Senoh, S. Nagahama, N. Iwasa, T. Yamada, T. Matsusita, S. S. H. Kiyoku, T. Kozaki, H. Umemoto, M. Sano, and K. Chocho, Appl. Phys. Lett. **72**, 211 (1998).
[6] P. Kozodoy, M. Hansen, S. P. DenBaars, U. K. Mishra, and J. Kaauffman, Appl. Phys. Lett. **74**, 3681 (1999).
[7] S. Nakamura and G. Fasol, *The Blue Laser Diode* (Springer, Heidelberg, 1997).
[8] M. Shiojiri, M. Čeh, S. Šturm, C. C. Chuo, J. T. Hsu, J. R. Yang, and H. Saijo, Appl. Phys. Lett. **87**, 031914 (2005).
[9] M. Čeh, S. Šturm, H. Saijo, J.-T. Hsu, J.-R. Yang, and M. Shiojiri, in Proceedings of European Microscopy Conference 2004, Antwerp, 2004, MS03.06.
[10] F. A. Ponce, J. S. Major, W. E. Plano, and D. F. Welch, Appl. Phys. Lett. **65**, 2302 (1994).
[11] F. Ponce, D. Chen, W. T. Young, J. W. Steeds, and S. Nakamura, Mater. Res. Soc. Symp. Proc. **449**, 405 (1997).
[12] P. Vennéguès, B. Beaumont, M. Vaille, and P. Gibart, Appl. Phys. Lett. **70**, 2434 (1997).
[13] X. H. Wu, C. R. Elsass, A. Abare, M. Mack, S. Keller, P. M. Petroff, S. P. DenBaars, and J. S. Speck, Appl. Phys. Lett. **72**, 692 (1998).
[14] Y. Chen, T. Takeuchi, H. Amino, I. Akasaki, N. Yamada, Y. Kaneko, and S. Y. Wang, Appl. Phys. Lett. **72**, 710 (1998).
[15] N. Sharma, P. Thomas, D. Tricker, and C. Humphreys, Appl. Phys. Lett. **77**, 1274 (2000).
[16] Z. Liliental-Weber, Y. Chen, S. Ruvimov, and J. Washburn, Phys. Rev. Lett. **79**, 2835 (1997).
[17] K. Watanabe, J. R. Yang, S. Y. Huang, K. Inoke, J. T. Hsu, R. C. Tu, T. Yamazaki, N. Nakanishi, and M. Shiojiri, Appl. Phys. Lett. **82**, 718 (2003).
[18] H. Saijo, J. T. Hsu, R. C. Tu, M. Yamada, M. Nakagawa, J. R. Yang, and M. Shiojiri, Appl. Phys. Lett. **84**, 2271 (2004).
[19] R. C. Tu, W. H. Kuo, T. C. Wang, C. J. Tun, F. C. Hwang, J. Y. Chi, and J. T. Hsu, in *Proceedings of the Fourth International Symposium on Blue Laser and Light Emitting Diodes*, Cordoba, Spain, 2002, p. 1.
[20] R. C. Tu, C. J. Tun, J. K. Sheu, W. H. Kuo, T. C. Wang, C. E. Tsai, J. T. Hsu, J. Chi, and G. C. Chi, IEEE Electron Device Lett. **24**, 206 (2003).
[21] S. J. Pennycook and P. D. Nellist, *Impact of Electron and Scanning Probe Microscopy on Material Research* (Kluwer, Dordrecht, 1999), 161–207.
[22] M. Shiojiri and H. Saijo, J. Microsc. (in press).
[23] K. Watanabe, J.-R. Yang, N. Nakanishi, K. Inoke, and M. Shiojiri, Appl. Phys. Lett. **80**, 761 (2002).
[24] L. T. Romano and J. E. Northrup, *Properties, Processing and Applications of Gallium Nitride and Related Semiconductors* (INSPEC, London, 1999), pp. 226–229.
[25] K. Watanabe, N. Nakanishi, T. Yamazaki, J. R. Yang, S. Y. Huang, K. Inoke, J. T. Hsu, R. C. Tu, and M. Shiojiri, Appl. Phys. Lett. **82**, 715 (2003).
[26] F. C. Frank, Acta Crystallogr. **4**, 497 (1951).
[27] J. E. Northrup and J. Neugebauer, Phys. Rev. B **60**, R8473 (1999).
[28] P. D. Brown, J. Cryst. Growth **210**, 143 (2000).
[29] K. Hiramatsu, K. Nishiyama, A. Motogaito, H. Miyake, Y. Iyechika, and T. Maeda, Phys. Status Solidi A **176**, 535 (1999).

Downloaded 11 Sep 2008 to 140.112.113.225. Redistribution subject to AIP license or copyright; see http://jap.aip.org/jap/copyright.jsp